J Mater Sci (2011) 46:6172–6190
DOI 10.1007/s10853-011-5688-0

ABBASCHIAN FESTSCHRIFT

The description of morphologically stable regimes for steady state solidification based on the maximum entropy production rate postulate

J. A. Sekhar

Received: 12 December 2010 / Accepted: 2 June 2011 / Published online: 7 July 2011

Abstract The maximum entropy production rate (MEPR) in the solid–liquid zone is developed and tested as a possible postulate for predicting the stable morphology for the special case of steady state directional solidification (DS). The principle of MEPR states that, if there are sufficient degrees of freedom within a system, it will adopt a stable state at which *the entropy generation (production) rate* is maximized. Where feasible, the system will also try and adopt a steady state. The MEPR postulate determines the most probable state and therefore allows pathway selections to occur in an open thermodynamic system. In the context of steady state solidification, pathway selections are reflected in the corresponding morphological selections made by the system in the solid–liquid (mushy) zone in order to cope with the required entropy production. Steady state solidification is feasible at both close to, and far from equilibrium conditions. Based on MEPR, a model is proposed for examining the stability of various morphologies that have been experimentally observed during steady state directional solidification. This model employs a control volume approach for entropy balance, including the entropy generation term (S_{gen}), which depends on the diffuse zone and average temperature of the solid–liquid region within the control volume. In this manner, the model takes a different approach from the successful kinetic models that have been able to predict key features of stable morphological patterns. Unstable planar interfaces, faceted cellular arrays, cell–dendrite transitions, half cells both faceted and smooth, and other transitions such as the absolute stability transition at high solid/liquid velocities are examined with the model. Uncommon solidification morphological features such as *non-crystallographic* dendrites and discontinuous cell-tip splitting are also examined with the model. The preferred morphological change-direction for the emergence of the stable *morphological* feature is inferred with the MEPR postulate in a manner analogous to the free energy minimization principle(s) when used for predicting phase *stability* and metastable phase formation. Aspects of mixed-mode order transformation characteristics are also discussed for non-equilibrium solidification containing a diffuse interface, in contrast to classifying solidification as purely a first order transformation. The MEPR model predictions are shown to follow the experimental transitions observed to date in several historical studies.

List of symbols

A	Area of interface (m^2)
A_f	Affinity (J/mol)
C	Composition (mol/m^3)
C_e	Eutectic composition (mol/m^3)
D_l	Solute diffusivity in the liquid (m^2/s)
D_{avi}	Average solute diffusivity in the interface or mushy zone regions (m^2/s)
G_T	Diffuse zone temperature gradient (K/m)
G_{T_s}	Temperature Gradient in the solid (K/m)
G_{T_l}	Temperature Gradient in the liquid (K/m)
K_{av}	Average thermal conductivity in the mushy zone
k	Partition ratio (dimensionless)
m_l	Slope of liquidus (K m^3/mol)
T_{av}	Average temperature between T_l and T_s (K)

J. A. Sekhar (✉)
Materials and Innovation Sciences Division, MHI Inc., Cincinnati, OH 45215, USA
e-mail: sekharja@ucmail.uc.edu

J. A. Sekhar
Materials and Energy Program, University of Cincinnati, Cincinnati, OH 45221-0012, USA

t	Time (s)
T_l	Liquidus temperature (K)
T_s	Solidus temperature (K)
T_m	Melting temperature (K)
R_g	Molar gas constant (8.314 J/mol K)
R	Volumetric gas constant (R_g/v_m) (J/m^3 K)
v_m	Molar volume (m^3/mol)
ΔC_o	Equilibrium concentration difference between the liquidus and solidus at the solidus temperature of an alloy (mol/m^3)
Δh_{sl}	Equilibrium value of latent heat per unit volume (J/m^3). Note that the sign convention used is the casting literature convention further explained in footnote 2
ΔT_i	Undercooling $\sim$ (T_l - T'_o (C_o)) (K)
ΔT	(T_l - T_s) (K)
T'_o (C_o)	Locus for equi-chemical potential line in the phase diagram [124]
ΔT_o	$m_l \cdot \Delta C_o$ (K)
dS_{gen}/dt	The rate of entropy production or generation (J/K s)
ds_{gen}/dt	The rate of entropy production or generation density (J/m^3 K s)
S_{gen}	Irreversible Entropy Generated (J/K s)
S	Entropy (J/K)
s	Entropy per unit volume (J/m^3 K)
Δs_{sl}	Equilibrium value of entropy change during solidifcation per unit volume (J/m^3 K)
$\check{s}_{sl}$	Molar entropy (J/mol K)
V	Steady state velocity (m/s)
V_c	Critical velocity for planar to cell transition (m/s)
W	Work (J)
MEPR	Maximum entropy production (generation) rate density (J/m^3 K s)
PPEDMR	Prigogine Principle of Entropy Dissipation Minimization Rate

Greek symbols

α	Lattice parameter (m)
ζ	Diffuse interface distance (>10^{-9} m for metals) also equal to $\sim$ $\Delta T_o/G$ for the mushy zone for metals
δ_c	Solute boundary layer
ψ	Clubbed force–flux entropy production rate/unit volume (J/m^3 K s)
ν	Jump frequency from liquid to solid at a temperature T_{av} (s^{-1})
ε	Net distance moved by the interface when 1 mol of atoms transform to the solid from the liquid (m)
ω	Energy of defects per unit volume (J/m^3)
γ_{gb}	Grain boundary energy (J/m^2)
λ	Intercellular or interdendritic primary spacing (m)
χ	Morphology parameter that depends on G_T and T_{av} and composition
$\Delta\mu_{sl}$	Free energy/mole (J/mol)
$\Delta\mu_c$	Driving force per mole (J/mol)
$\Delta\check{s}_{sl}$	Molar entropy of solidification (J/mol·K)

Subscripts

cv	Control volume
sl	Solid–liquid

Introduction

The morphological evolution sequence and the length scales of solidification structures (patterns in the microstructure) that form as a consequence of freezing of a liquid are now known to a great degree [1–4].[1] Solidification microstructure formation by the controlled lowering of the temperature of a liquid, whether performed in a directionally solidified temperature gradient furnace (DS) or by the controlled bulk cooling of the liquid, is a well studied problem [1–66]. Solidification is an important transformation both from a technological viewpoint and for broad scientific exploration considerations. Solidification studies have yielded important material-specific parameters. For example, solidification in microgravity conditions has been used [1–4, 49–51] to determine accurate diffusion constants in the liquid when buoyancy driven fluid flow velocities become smaller than 1 μ/s. The as cast microstructure scale, is also directly related (empirically) to several important engineering properties in a multitude of applications which range from electronics to jet engines.

There are by now a number of studies starting with Dash [15], Jackson [66], and others [1–4, 21, 41, 42, 47, 52] on morphology and defect evolution, mostly in the context of growing defect-free crystals. Removing defects from seed crystals and growing as slowly as possible (well below interface break down velocities) gives rise to crystals with the least boundary type defects. Residual stresses may cause oscillations in the interface growth rate [41–43, 47]. Preventing the buildup of residual thermal stresses and reducing convection by imposing external magnetic fields and modifying temperature gradients [1–4, 21, 42, 47, 53] prevents cracks and solute banding. The presence of facets when seen along with curved surfaces together in an evolving solid microstructure also leads to unpredictable segregation (banding) and related defects [3, 4, 14, 15].

Although morphological bifurcations are recognized and well studied during solidification, especially with transparent metal analogs and other modeling based imaging techniques, [1–11, 32–47, 58–62] there is no overriding principle or empirical correlation that adequately predicts

[1] The first four references cited as Refs [1–4] are the main textbooks with select primary articles for solidification that I use in my *Introduction to Solidification* course.

an *overall* stable morphology when the patterns become complex. However, this is not to say that the field is bereft of descriptive models. Several kinetic models offer very reasonable predictions of key features like the interface stability or the tip radius of a dendrite [1–49, 63–67]. In most kinetic modeling for microstructure predictions, local equilibrium at the transforming solid–liquid interface is a key assumption [1–11, 25–47]. The consequences of relaxing this assumption by invoking changes in the partition coefficient(s) as a continuously varying function of velocity is also by now a reasonably well developed method in as far as predicting the resultant non-equilibrium microstructure for several alloy systems [1–11, 23–27, 68].

Kinetic and empirical models have great value. The very successful correlation between secondary dendrite arm sizes for equiaxed castings to the cooling rate has enriched the casting industry. However, again there is no overriding principle that describes the formation of DS microstructures (and defects) *especially* when cellular morphologies, are noted during directional solidification (positive temperature gradient) conditions. Figure 1 [64, 65, 69–78] shows pictures of typical steady state morphological variations that have been observed in transparent DS experiments with metal analogous. Although great strides have been made [1–51, 53–67, 69–123] for predicting the scale of microstructures, the required understanding is still far from optimal.

This article[2] presents a new entropy based approach to complement the existing kinetic approaches. Historically, the overall solidification morphology has not been comprehensively studied from this point of view of entropy generation (dS_{gen}/dt), except by Kirkaldy and a few others [5–7, 94]. However, a gradient energy approach which contains S_{gen} from the free energy dissipation (gradient energy) is commonly used along with an order parameter in a popular numerical technique known as the phase field method. Such an approach uses the Ginsberg and Landau [55] and Cahn et al. [32–36, 56, 122] developed techniques for spinodal development and extends predictions made by kinetic models such as the tip stability for shape prediction capabilities [1–4, 13, 14, 16–29, 32–36, 54–56, 93, 121–123]. Entropy is a non-conserved quantity but can be rigorously treated in phase field approaches by using the Allen–Cahn approach [35]. The problems with the phase field approach lies in identifying an order function that has an adequate theoretical basis [5–7, 35, 108–111].

The MEPR may also allow predictions of morphology [5–7]; however, it appears the MEPR, which is applicable in many diverse fields (e.g., climate prediction, cell biology, etc.) [5, 6, 111, 112] can make predictions based only on a maxima. In the materials' literature, such maxima based predictions may be traced to the Zener model [13] and later studies by Trivedi, Kurz, Ben-Jacob et al. and others [1–4, 8, 16, 17, 64, 106, 110, 121, 123].

There is some doubt as to which extremum principle, if any, could be valid for dendrites [1–17]. In contrast, the linear stability approaches have predicted a better fit with experimental data [1–4, 15–26, 93, 106, 108, 122, 124, 125]. However, it appears that rigorous and unique solutions also may not always be possible to infer from linear stability principles for many conditions of solidification, unless anisotropy and shrinkage velocity are considered [126]. There is a difference in the matching ability between experiments and models for dendrites that grow in a positive temperature gradient and those that grow in a negative temperature gradient condition; the latter has proved tougher to match. It has not been possible to adequately match theory and experiments for the dendrite tip radius [126]; even if a correction term for the energy conservation equation (Stefan equation) is employed at a solid-liquid interface that includes shrinkage. Regardless, prediction of the dendrite tip radius as a function of the tip solidification velocity do not also appear to follow any *known* extremum models when compared with experimental observations. Coupled structures are more aligned with extremum models, e.g., the eutectic phase lamellar spacing's [1–4, 8, 12–14, 93]. In contrast, for chemically reacting systems, where there is a strong reaction affinity or a presence of other strong potential gradients, there is some evidence of the new principles of maximum entropy generation rate as applicable for inferring some of the morphological patterns and pathway selection features [51, 53–62, 79–112, 122] that emerge from chemical reactions. In fact, there is a significant richness in morphological complexity that is feasible with changes in the rate of entropy generation in chemical reactions [51, 53–62, 69–71, 79–111, 118, 119].

In this article, we study entropy production rate (ds_{gen}/dt), free energy dissipation, and entropy transfer (net export of entropy from a control volume) to possibly infer a common principle for morphological development of the solid–liquid interface at steady state conditions, across several length scales of the solidification problem. The control volume approach is used for entropy balance, shown in Fig. 2. This approach makes the problem less complex to formulate and, as discussed in this article below, is able to verify the most stable *overall* shapes reported in several published reports [1–123, 127, 128]. An attempt is made in this article to describe such morphological features and morphological transitions with the entropy rate maximization postulate. For Bridgeman type DS, the controlling parameters for morphological stability are historically thought to be the velocity of solidification (V), composition (C_0), and temperature

[2] Note that capital letters are used for the extensive quantity and lower case letters for the extensive quantity per volume. Example, S_{gen} (entropy generation rate) has units of J/K s and correspondingly s_{gen} has units of J/K s m^3. Molar entropy is š (J/mol K). In this article dS_{gen}/dt is used as the symbol for entropy generation.

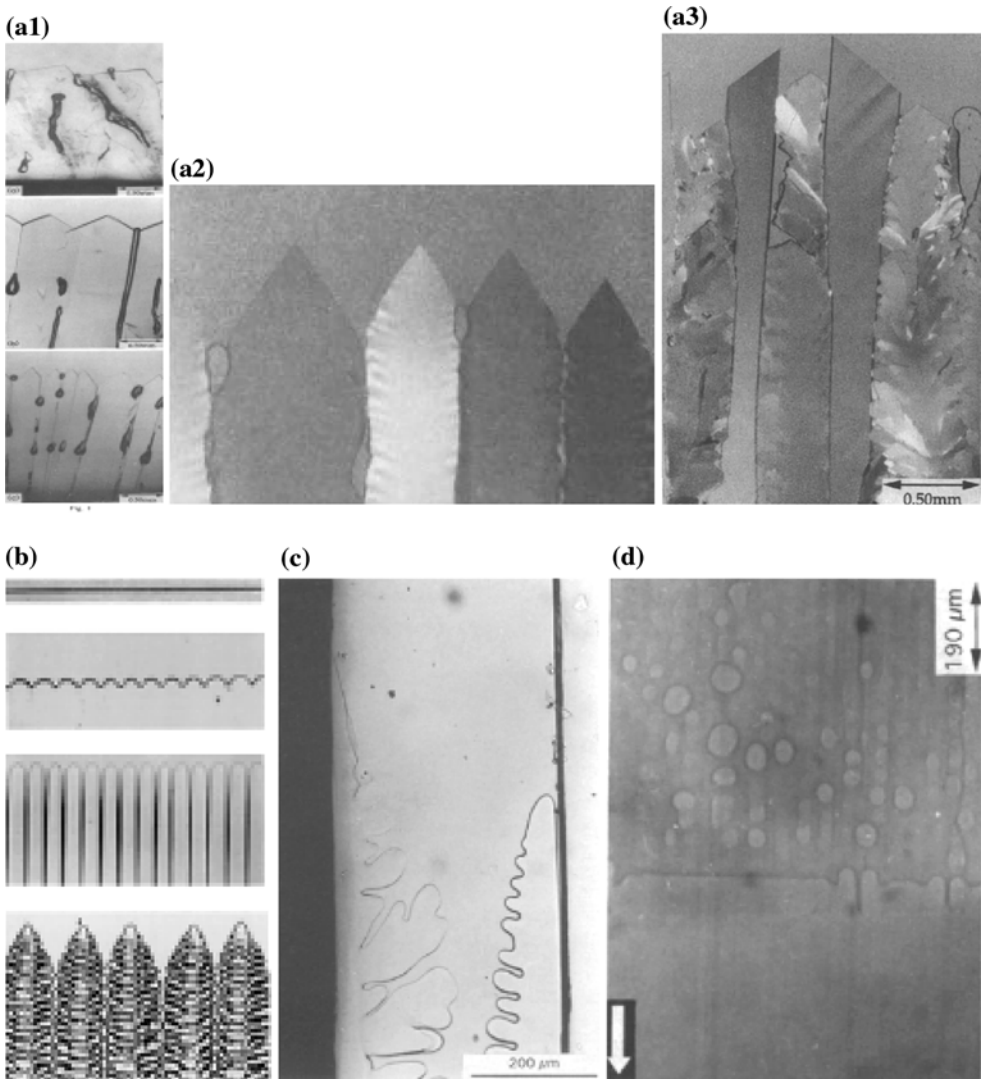

Fig. 1 Shapes of solid–liquid interfaces in salol (**a1**–**a3**) [41, 42] and from various SCN experiments (**b**–**d**). **a1** Shows from top to bottom the tip angle reduction with an increase in the velocity, **a2** the development of secondary arm facets, **a3** half facet cell arrays possibly with stress related birefringence patterns. **b** The transformation sequence in a succinonitrile alloy (SCN alloy), with an increase in the velocity (top to bottom) showing the change from a plane front to stubby cells to deep cells to deep dendrites; heat flow direction is from top to bottom of the pictures [1–4, 11, 63, 64] (this picture was deemed to be in the open literature and no permissions for publication ware sought, a situation that can be corrected if required).; Typical temperature gradient and interface velocities are in the order ∼5 K/mm and 10 μm/s, respectively. **c** Half cells and dendrites in SCN alloys (note also the breakdown at the grain boundary regions) [69, 70] and **d** equiaxed transitions in SCN alloys [71]. In **b** the spacing of cells decreases first with an increase in the velocity (stubby to deep cells) and then increases with velocity as the dendrite bifurcation is encountered. One should note that at a extremely high velocities ∼0.1–1 m/s, a plane front like flat interface is again observed [10, 72]. Other morpholgies similar to **a3** have also been reported in the literature such as half cells and confused structures that continuously split at the tip regions. Such structures are also noted during morphological transitions from cells to dendrites when channels or small insoluble solid particles are encountered by an advancing s/l interface [9, 73, 110]. Except for a3, all other shapes were photographed at steady state conditions

gradient G_{T_s}. The rate of entropy generation ($\mathrm{d}s_{\mathrm{gen}}/\mathrm{d}t$) can also be varied by altering these three parameters.

The solid–liquid interface transition region is commonly referred to as atomistically sharp when the dimensionless entropy of transformation (mentioned above) is larger than ∼2 [66]. It will be shown below that the MEPR model includes this term in the new equation for interface instability. (Dimensionless entropy is $\Delta\check{s}_{\mathrm{sl}}/R_{\mathrm{g}}$, where $\Delta\check{s}_{\mathrm{sl}}$ is the entropy per mole for the liquid–solid transformation, and R_{g} is the universal gas constant.) Such interfaces, during DS growth, display facets (when observed at the resolution of micrometers) in contrast to interfaces that are diffuse (i.e., atomistically rough) which display more well defined curved smooth features, again when observed at the scale of the optical microscope resolution. Closed packed planes retain the plane front interface (i.e., have higher stability with

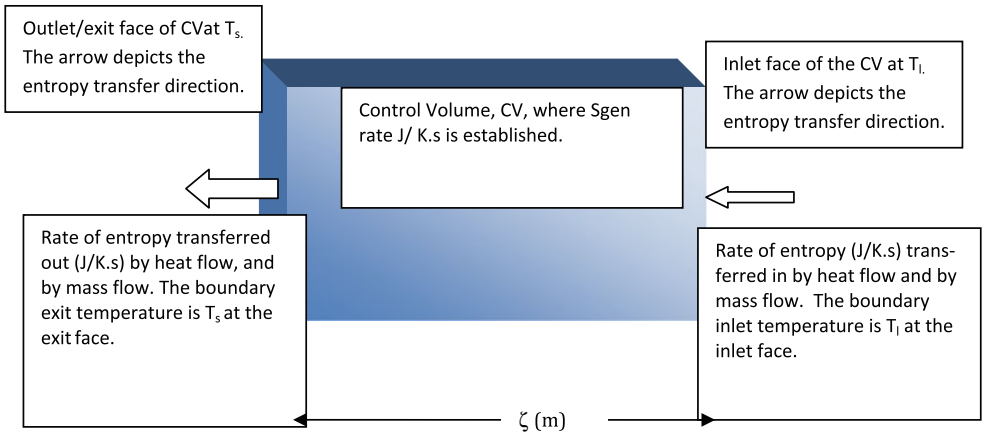

Fig. 2 An explanation of the control volume approach for entropy balance. The *shaded area* is the interface region where the entropy is generated. During solidification, the CV moves with a fixed velocity from left to right. Thermal and other potential gradients are established. ζ (the extent of the control volume) is the diffuse interface or mushy zone distance. The $x = 0$ is co-located with T_s

increasing velocity of solidification) for the same conditions of imposed growth, compared to less closed pack planes [113]. Although faceting and sharp interface structures are associated with a high entropy of transformation, Cahn [65] has correctly pointed out that the diffuseness of an interface is a function of the velocity of the interface (velocity is related to the driving force and therefore increases the probability to overcome the activation energy barrier for solidification). Hence facet to non-facet transitions are expected to occur. Experiments have confirmed such facet to non-facet transitions with an increase in the velocity [1–4, 31, 39–44] for a number of materials that are associated with a high entropy of solidification transformation. The model developed below also explains such transitions.

Interface instability (bifurcation from plane front to wavy instabilities with increasing velocity) is possible during DS [1–7, 66, 77, 78, 113], with the instability bifurcations being first observed in regions close to existing high angle boundary features in the solid [78]. For dilute binary alloys that have a low dimensionless entropy of transformation, the transitions that are noted with an increase in velocity take the form of an initially plane front interface that changes to a stubby cellular pattern, then to deep cells, then to preferred crystallographically oriented dendrites, to deep dendrites with well developed secondary arms, then to very fine plane front like fine cellular structure at high velocities (high Peclet number absolute stability conditions) [1–10, 24, 65, 74]. When physical constraints like wetting surfaces, particles or small channels are introduced in the solidifying volume, unique morphologies such as half cells and half dendrites or even equiaxed growth, ahead of the solid/liquid (s/l) interface is observed [9, 69–74].

To date, all models that can predict solidification structure (morphology) use the solid/liquid surface energy as an import parameter which often defines the scale of the resultant microstructure. However, if the interface has characteristics of a second order transformation, then the use of an s/l surface energy is troublesome because the term essentially comes from a volume free energy in the diffuse region. The melting point is affected by defects and curvature both which are a priory not known. We will overcome the use of a solid–liquid interface energy and the melting point by considering the interface region of dimension (ζ, m), bounded by the isotherms T_s and T_l and separated by $\Delta T = (T_l - T_s)$. For DS conditions *with an independently fixed velocity* (V) *and independently fixed linear temperature gradient* (G_T), we will consider $G_T = \Delta T/\zeta$ as being linear across ζ. A one-dimensional system is considered. The system is comprised of the region between the fixed boundary control volume (i.e., contains the s/l region) when identified in the mushy zone for alloys. The control volume extends up to, but not beyond, the rigorous solid and rigorous liquid states (see Fig. 2). The steady state of a system is reached when the entropy rate change averaged over sufficiently long times vanishes at all positions ($(\mathrm{d}s/\mathrm{d}t)_x = 0$). At the steady state, the entropy production within the system is equal to the net entropy export.

The diffuse interface region, even when planar conditions are noted between the rigorous solid and rigorous liquid phases, is not only as a useful convenience for numerical methods (e.g., the phase field approach [17–27]) but as we will show below, is a region important to entropy production. Note also that $(\mathrm{d}F/\mathrm{d}T)_v = -S$. As the specific heat at constant volume is a positive quantity (required for material stability), S is always positive and the slope of the F vs. T curve has to have a negative value. As discussed by Cahn [65], $\mathrm{d}F/\mathrm{d}x$ (where positive x is the opposite direction to the heat flux, and F is the Helmholtz free energy) has an overall slope such that $\mathrm{d}F/\mathrm{d}T$ is always negative at any

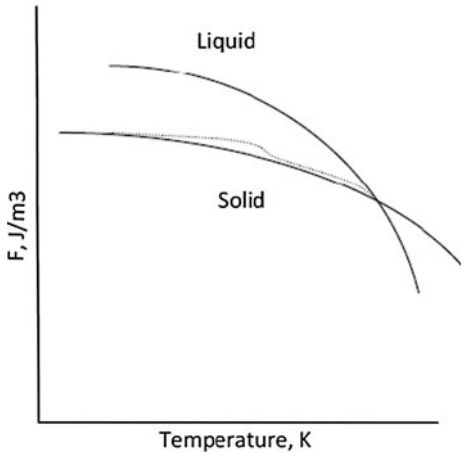

Fig. 3 A plot of free energy (F) vs. T (or distance assuming liquid is on the right and heat flows to the left in a one-dimensional problem see Fig. 2). The *solid line* is the defect-free solid. The *dotted line* is the defect containing solid. Several free energy configurations are possible in the diffuse region which caters to the overcoming of the activation energy experienced by a rigorous liquid atom to transfer to the rigorous solid state. The figure illustrates a shape of the free energy vs. temperature that does not conflict with $[dF/dT]_P = -S$ with a overall negative slope in the free energy curve, a shape that could invoke a separation or describe a critical point type phenomena that is possible which will further increase the undercooling as well as S_{gen}, yet maintain overall $[dF/dT]_P$ to be always $= (-S)$. Note that $[dF/dx]_T$ and $[dF/dT]_x$ within the diffuse zone could be zero (i.e., locally $(\Delta H/T) = (\Delta S)$) or change to a higher entropy production configuration. Depending on the type of molecule that is solidifying, especially when molecules have considerable rotational energy (e.g., super-lattice forming plastic crystals), metastable states may also be present where the configurational heat capacity has not attained its full value, thereby making C_p smaller than the equilibrium value. This will influence K_{av}. The distribution of liquid and solid clusters in the diffuse zone has been modeled with density wave theories and molecular dynamic studies [30, 120, 131] for nucleation and growth that show tiny clusters of rigorous solid and rigorous liquid mixed together in the interface region. Similar molecular dynamic reports in the presence of a strong temperature gradient are not available. When a free energy reduction is possible at an undercooling, this free energy can be used for internal work production

location x. Figure 3 shows a schematic of a possible variation of F within the diffuse interface. Note that in Fig. 2 the $x = 0$ is co-located with T_s. One of the major leaps of faith in this article with the proposed new dS_{gen}/dt approach is that interface diffuseness can be replaced by the mushy zone distance for an alloy. When considering dilute alloys, the mushy zone thickness replaces the interface diffuseness, irrespective of any normalization by the characteristic length scale of the solidification problem.

Order of transformation and the origin of a diffuse interface

If energy is added uniformly in the form of heat, to a solid at its melting point the only option for the solid is to absorb the energy by breaking symmetry, which results in melting (lowering viscosity, increasing relaxation speed of molecules [68, 115, 128], volumetric expansion, etc.). This change of internal structure is also a manner in which the specific heat is discontinuously adjusted at the melting interface by the change of phase [99]. An increase in pressure normally increases the melting point, depending on the change in molar volume [1–4, 37]. Melting and solidification at close to equilibrium conditions are reviewed in Refs. [1–7, 52, 68, 115, 120–123, 127, 128] also revealing the very classic issues that trouble our understanding of this process [120].

Solidification is historically referred to as a first order transformation, i.e., a transformation where the first derivative of free energy per mole is discontinuous at the melting point. Yet, as noted above, a diffuse interface is well recognized as a distinct possibility during solidification [65, 126]. Based on the molecular modeling studies of the transforming region [30]; the measurement of the interface Seebeck coefficient by Abbaschian et al. [31, 113]; and the success of phase field models discussed above, it could be considered that solidification dynamics is better understood by thinking of the transformation to be a mixed, first *and* second order phenomena at the transforming interface region, i.e., with a discontinuity only in the second derivative of the free energy, yet producing heat during the s/l transformation. This strict categorization as a first or second order transformation is important, though not essential, to our discussions below. We will consider the change-over region between liquid and solid to essentially have a finite dimension over which a temperature gradient and other gradients are established. We will assume that a non-linear free energy curve is established in the diffuse interface region. Note that diffuse interfaces may be described by a double well energy approach [126] which is also shown in the dashed line in Fig. 3. More importantly it is possible that a region where $d^2F/dx^2 = 0$ may exist, which can indicate critical point like ambiguity inside the interface phases, thus allowing for the development of spinodal like fluctuations and transformations. The shape of this free energy variation will be important in determining the features of the rigorous solid-like and rigorous liquid-like distribution across the diffuse interface region (Fig. 3). The mixing of these regions also produces entropy when rearranging the distribution and thus support defects as an outcome of the rearrangement. Depending on short range liquid clustering tendencies; the activation energy barrier (inclusive of diffusion activation in the liquid) for an atom to go from liquid to solid; the presence of defects such as dislocations, vacancies, twins, and the energy of *solid–solid* grain boundaries (whether high energy (typically greater than 100 mJ/m^2) or low energy (typically $\sim$10 mJ/m^2)) that may form and be retained in

the final solid as a result of solidification; there is thus a wide variation of possible microstructures and nanostructures [105–107] that may be observed in the final residual solid. This is analogous to clustering and self-ordering phenomena during a spontaneous reaction transformation. In this manner work can be done by the system yet increase the entropy to a maximum allowable level.

Describing any process as reversible, implies that the work done is equal to conversion of the maximum possible available work potential and that $S_{gen} = 0$. A process is reversible primarily because there is no change in the Gibbs or Helmholtz (G, F) free-energies and $S_{gen} = 0$ for the process. However, for phase change processes such as solidification, the latent heat is generated at T_m and the material changes from rigorous liquid to rigorous solid at T_m. For a first order, internally reversible transformation, the melting and solidification happens at the melting point (single temperature), consequently the maximum spontaneous work possible from the solidification process at T_m can only be zero (Carnot Efficiency also shows that $((1 - T_m/T_m) = 0)$. For the case of a dilute interstitial type alloy, the excess entropy in the liquid correspondingly is captured by the change in the melting point. For completeness, it should be understood that, the exergy (i.e., the work potential when referenced to a base temperature T_o, other than T_m) of a liquid is higher than that of the solid at the melting point. This happens because at a downstream temperature, the latent heat may be converted partially to work by enabling internal processes in the solidified material or by an appropriately configured heat engine.

As discussed above, the activation energy barrier that may be required to be overcome by an atom or molecule to change from being associated with a rigorous liquid condition to a rigorous solid condition has to be enabled by a force (i.e., chemical potential gradient [115, 122]), and consequently there is the possibility of entropy generation from the force–flux (transformation flux) relationship that is similar to that of a chemical reaction. There may be other force–flux conditions present also. These are discussed later in this article. The possibility of force and conjugate fluxes during solidification cannot support a reversible transformation and hence cannot support the concept of a first order transformation. Consequently the diffuseness is a natural development across a solid–liquid zone.

Entropy Balance Method, MEPR, and the Prigogine Principle

Metastable states and several 'natural' steady states are feasible when free forces exist in a system. The principle of MEPR states that, if there are sufficient degrees of freedom within the open system, then a perturbation of the system, will take the system towards a final steady state at which the rate of S_{gen} production (dS_{gen}/dt) is maximized *compared to other possible steady states*. For a change in the imposed steady state variables during DS, a new rate of s_{gen} is established by different force–flux combinations. The Prigogine principle of entropy *minimization rate* (PPEDMR) [82, 83, 115] for a system undergoing irreversible entropy production while approaching equilibrium conditions is fully compatible with the postulate for the maximum entropy production rate MEPR. PPEDMR leads the system to an equilibrium state for an isolated system by choosing a MEPR determined pathway. MEPR can lead to a steady state for a system which is attempting to lower its entropy generation rate. At a steady state the differential $d(s_{gen})/d(\text{flux})$ for all fluxes is zero which satisfies both the PPEDMR and the MEPR. The available conditions for free forces and fluxes then determine whether the second differential is positive or negative or zero. When zero, internal work is feasible. The principle of MEPR states that, if there are sufficient degrees of freedom within a system, it will adopt a stable state at which *the entropy generation (production) rate* is maximized. Whenever feasible the system will also try and adopt a steady state condition. MEPR determines the most probable state. When entropy is produced locally (example by a reaction), it is either exported away from the local production location or accumulates. Diffusion of matter or heat by a conjugate force–flux combination generates additional entropy. Entropy exchange can also occur reversibly without generating entropy. The MEPR principle looks for the pathway selection which allows the entropy generation *density* to be maximized and so must be considered at all locations. A transformation within an isolated system, or within a closed system or an open system will display different aspects of MEPR. For a steady state closed or open system, entropy will be generated and transferred (net export or import) across the system boundaries at the same rate. For an isolated system within which a chemical reaction can occur, diffusion processes for heat or mass will internally equilibrate the isolated system and the MEPR principle for the isolated system will determine the rate at which fluctuations relax thereby providing the most optimal pathway. Steady states may be established as a feature of the MEPR. For a closed or open system the rate of approach to equilibrium or to a steady state condition of the system after an external exchange event has occurred is governed by the rate of entropy transported across the system boundaries and the rate of irreversible entropy production on account of any fluxes developed in the system. Figure 4 shows typical entropy generation rate pathways starting from a perturbed state. If the system is allowed to equilibrate in temperature, pressure and chemical potential across the boundaries then with time, the dS_{gen}/dt will become zero

(PPEDMR). However, MEPR will determine the overall rate for all locations in the system and therefore the total pathway for the system. Depending on the constraints the Prigogine principle (PPEDMR) may ensure that the rate of entropy generation is minimized also with respect to the fluxes (Fig. 4a) [109–112]. The steady state conditions are shown in Fig. 4b and c that are applicable for open and closed systems with continuous exchange at the system boundaries. Figure 4d shows the possibility of steady state conditions within an isolated or closed system which maximizes entropy with a short 'natural' steady state period. Note also the wavy nature of the pseudo steady state which is one way in which PPEDMR and MEPR principles can 'interact' and thus can lead to oscillations especially BZ oscillations [57, 96, 97]. The particular maximum entropy generation condition from several conjugate force–flux fluctuation possibilities is discussed in Refs. [7, 97–99, 111, 115]. Figure 4e & f indicate how a steady state ds_{gen}/dt and maximum S_{gen} are developed across a conducting solid placed between two temperature reservoirs.

Figure 4a–f illustrate PPEDMR and MEPR for a displaced system that relaxes to a new state. For an isolated thermodynamic system, $dS/dt = dS_{gen}/dt$ and the maximum entropy production principle reveals the condition that an isolated system tends to a state of maximum entropy *along the fastest possible path.* The downward slope of ds_{gen}/dt is the PPEDMR and for a closed system, dS_{gen}/dt therefore becomes zero with time [115]. The Prigogine principle is easily shown to be applicable for any system that possesses sufficient degrees of freedom where the potential gradients will all tend to become very small or zero with time. The horizontal lines in Fig. 4, i.e., $ds_{gen}/dt =$ constant is the MEPR postulate when even comparisons are made between the several possible steady states, for example as compared in Fig. 4b and c where the horizontal lines are established at different ds_{gen}/dt. MEPR as noted in this article enables morphological pathway selections to be made for steady state conditions especially in open systems. However, MEPR is a postulate[3] that has not yet received universal acceptance and we examine it for the first time in this article for the special case of steady state Bridgeman directional solidification in order to describe the *overall* morphological feature stability.

It is by now well recognized that interfaces are often diffuse [122, 126, 131] when they are in motion, i.e., they change character from rigorous liquid to rigorous solid over a few atomic layers typically in the order of nanometers for simple metals and much larger for complex polymeric molecules. The conjugate force–flux conditions that become active now produce entropy (even a perturbation from equilibrium requires entropy generation to restore the entropy lost in order to reassert equilibrium). If there is a gradient of a potential and a conjugate flow across the diffuse region, even for a second order transformation (i.e., without heat production over the diffuse interface region), then there will be a corresponding entropy generation, S_{gen}, on account of the force–flux conditions. The reader is referred to [122] for details on the various force–flux relationships that are possible.

For an open system contained between fixed unchanging boundaries with balanced mass flows, the maximum possible non-boundary work is reflected in the change in the Helmholtz free energy (F) difference (ΔF) between the two rigorous states (i.e., rigorous liquid and rigorous solid in DS). For condensed systems we will consider the Helmholtz free energy (F) the same as the Gibbs free energy (G). Any internal or external work done therefore can be related to the work potential between the isotherms, i.e., within the bounding surfaces the volume. During DS there is an outflow of defects in the solid whether they are grain boundaries or dislocations or lattice defects. The maximum amount of stored energy at defects and interfaces created in DS processing can be enabled by a high $\Delta\mu_{sl} = (\Delta G_{sl}/\text{number of moles})$, wherever it happens in the solid–liquid region (s/l region) subject to second law restrictions on converting heat to work. ($\Delta\mu_{sl}$ is the change in free energy per mole between the rigorous liquid state and the rigorous solidified state.)

For a closed system, minimizing the rate of entropy production, (dS_{gen}/dt) with time for force–flux combinations, and maximizing the power output (for work), both push towards an operational efficiency [110], that is rarely encountered in spontaneously occurring processes in nature. Free (unfixed) thermodynamic forces in the system can, however, be mutually adjusted to bring the system to the state with a fixed entropy generation [111, 112, 114] but lower than that of the perturbed state. This is the Prigogine principle PPEDMR. The final entropy generation rate will be zero for a closed system and positive non-zero for an open system. For a steady state open systems, if we hypothesize that maximum entropy production rate (MEPR) maximizes the rate of entropy production (ds_{gen}/dt) between different steady state possibilities, this additional principle can guide the prediction of a particular steady state pathway. There is no other postulate but MEPR that allows a selection principle of the most probable pathway thus establishing morphology and defects between several possible pathways at steady state [111, 112]. For

[3] Although MEPR is a postulate, not yet completely verified in a universal sense, several authors consider the postulate to be tied to the second law of thermodynamics formulated by Gibbs–Claussius–Boltzman [6, 111, 125]. Martyushev et al. [6, 110] while crediting Ziegler [16] as being the first to propose a version of MEPR, also reason that if the entropy generation rate is at a maximum, then the second law statement by Claussius is necessarily closely related to MEPR.

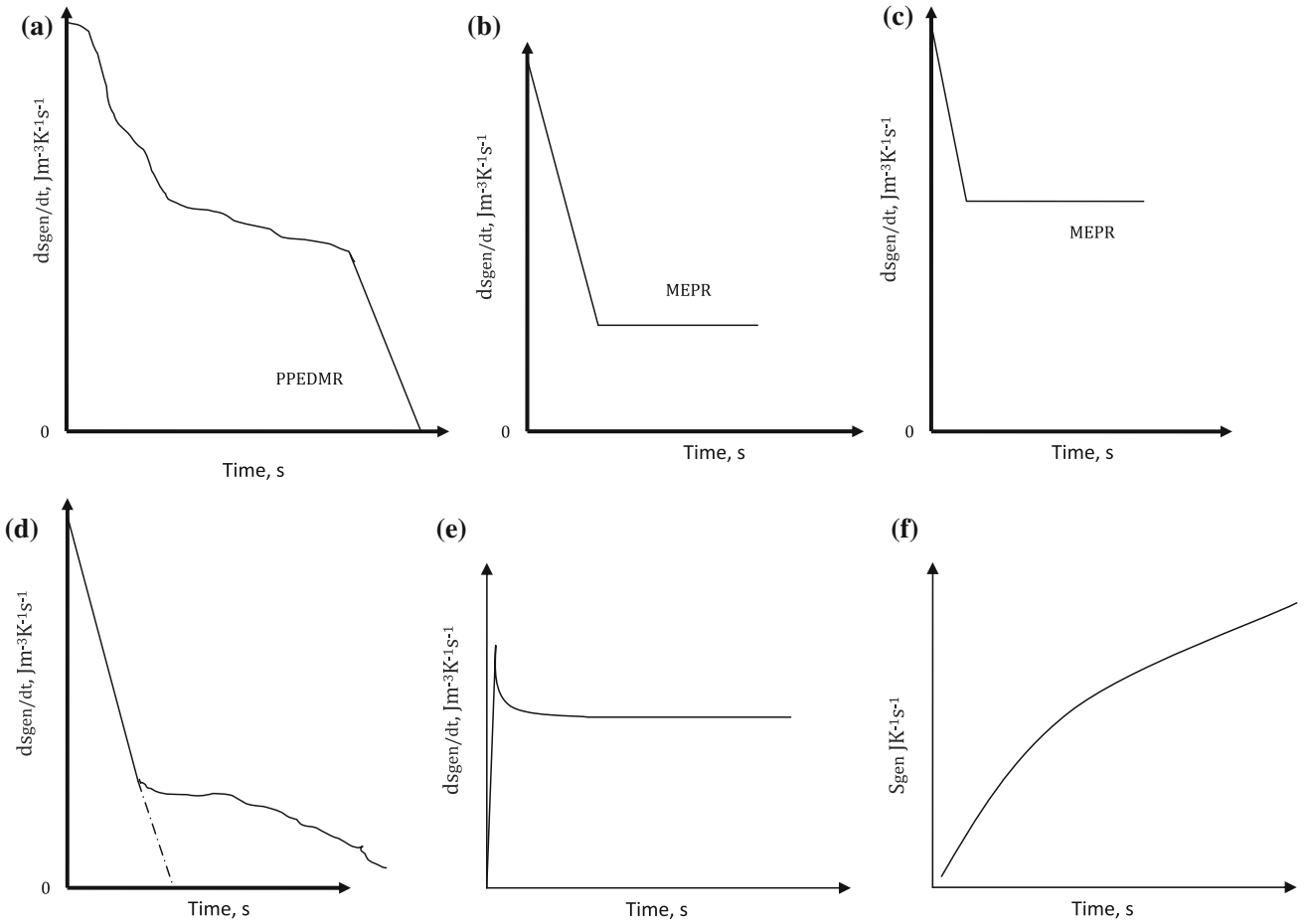

Fig. 4 **a**–**f** All illustrates PPEMDR and MERP in plots of *entropy production rate* as a function of *time* after perturbing a system to far from equilibrium conditions. The graphs illustrate what may happen to systems with time. **a**, **d** For closed systems, eventually the entropy production rate goes to zero with time; sometimes also encountering metastable steady states or pseudo steady states. The downward slope of the rate of S_{gen} is a reflection of PPEDMR. For a closed system dS_{gen}/dt becomes zero when free thermodynamic forces disappear. For open systems the rate of entropy generation at steady state is maximized for a given set of variables as per the MEPR hypothesis (compare *horizontal line* positions in **b** and **c**). Two possible steady states are shown by the *horizontal lines* in **b** and **c**. **b** A slower approach and lower S_{gen} rate at steady state whereas **c** shows a high rate approach to steady state and a higher S_{gen} rate at steady state. Equation 6a explains how different steady states may be reached. **e** The s_{gen} rate for any location inside a control volume where a temperature gradient evolves while steady state conditions are established (linearization) between two constant temperature reservoirs. The rate is maximized at the steady state condition. **f** The total S_{gen} in the system i.e. CV, that connects the reservoirs will increase with time. Note that there are no dominant free forces in **e** and **f** and both the MEPR and PPEDMR are applicable. Belousov–Zhabotinsky reactions may be noted as a feature for the type of oscillatory entropy generation rate behaviors shown in **a** or **d** [57, 80, 91, 114, 115]. The *dashed line* in **d** shows how a reaction which does not show a steady state would have progressed to a zero entropy generation condition in a closed system compared to when a pseudo steady state could be encountered as seen in **d**. At small deviations from equilibrium PPEDMR is a valid postulate. However MEPR is a more powerful postulate

steady state DS processing conditions, the entropy rate maximization hypothesis can be tested to compare the stability of all allowed solidification morphologies for various combinations of materials with different specific heats, velocity, and the temperature gradients for a Bridgeman type solidification situation.

Adding internal energy or transferring entropy by heat into a fixed volume increases the temperature of a region, as long as the volume is fixed. Note, however, for completeness that for some neutron stars, the addition of external (transferred) entropy can actually reduce the temperature, a consequence of energy–matter exchange in nuclear reactions in the presence of very strong gravity, thus sometimes leading to a '*negative*' specific heat in neutron stars. Negative specific heat is not considered in this article. Again depending on the complexity of molecules involved there is also a possibility that the configurational specific heat may not have also fully developed, thus temporarily reducing the specific heat because of the time constraints in fully establishing the equilibrium value or steady state values of

the specific heat. This possibility is also not considered. Figure 3, shows one possibility in the free energy profile for a diffuse interface. Note how a diffuse interface can itself span metastable states in order to reduce the overall free energy. If there is a continuous order or entropy parameter defined across the interface then the transformation is continuous as opposed to discontinuous transformations [99, 122]. We will assume continuity but do not necessarily have to do this with the control volume approach discussed below. In addition the MEPR can also test for intermediary metastable phases in the general manner discussed below with the control volume approach. Oscillatory conditions that mitigate the entropy exchange can arise from conditions similar to Belosouv–Zhabitonsky (BZ) reactions [53, 57, 79–91, 115] or with regions where entropy rate reduction occurs in a closed volume or steady state. These are shown in the various figures described in Fig. 4. Abbaschian et al. [26] have clearly noted oscillations in the Seebeck coefficient and in the measured interface temperature, even for a slow DS interface propagation ostensibly at steady state; while ensuring that convection is minimized. It is not clear if the residual stress states varied with time in their experiments, but it seems unlikely, and therefore the reasons for oscillations may have to do with BZ like adjustments within the interface [53–62, 79–109]. BZ conditions are not explored further in the rest of this article.

Entropy balance model

The control volume approach may be used for a one-dimensional formulation for entropy balance for a solidifying interface. The interface is bound by the control volume (CV) isotherms shown in Fig. 2, i.e., by T_s and T_l. As shown in Fig. 2. The entropy rate balance as given by:[4]

$$\mathrm{d}S_{cv}/\mathrm{d}t = \{\mathrm{d}S_{in}/\mathrm{d}t\,(\text{at the inlet isotherm}) - \mathrm{d}S_{out}/\mathrm{d}t\,(\text{at the outlet isotherm})\} + \mathrm{d}S_{gen}/\mathrm{d}t \quad (1a)$$

At steady state,

$$\mathrm{d}S_{cv}/\mathrm{d}t = 0 \quad (1b)$$

In the RHS of Eq. 1a, the first two terms arise from the entropy exchange by heat and mass flow at the CV boundaries, i.e., across the two isotherms for the one-dimensional formulation. S_{gen} or $\mathrm{d}S_{gen}/\mathrm{d}t$, is the irreversible entropy generation rate in the control volume (CV). As the rates of mass entering and leaving the CV are the same for steady state DS (assuming similar densities), all entropies can also be defined on a unit volume basis. Two balances may be made for the solidification control volume, namely, an energy balance that Δh_{sl} is scalar quantity in this article. The energy balance gives $\Delta h_{sl} = \Delta h_m + \omega$ where Δh_m is the latent heat with defects and ω is the energy of the defects per unit volume. The exit from the CV at the lower temperature isotherm is a defect containing solid, i.e., with a higher free energy and entropy per unit volume compared to a defect-free solid. The second is the entropy balance. The inlet entropy into the CV per unit volume is the liquid entropy at T_l, i.e., $(s_s + \Delta h_{sl}/T_m)$.[5] The exit entropy is closely approximated by the defect-free solid entropy plus the heat exchange entropy leaving the CV at T_s, i.e., $(s_s + \Delta h_m/T_s)$ plus $\mathrm{d}(S_{gen})/\mathrm{d}t$, i.e., the entropy generated in the CV.

In Eq. 2a, the symbol A is used for the solid–liquid interface area normal to the DS direction, and V is the steady state velocity. By fixing a coordinate system ($x = 0$) to the T_s isotherm (exit isotherm of the control volume) and V (m/s) as the steady state velocity, the following approximate expression for the entropy balance may be written;

$$\mathrm{d}S_{cv}/\mathrm{d}t = AV\Delta h_{sl}/T_m - AV\Delta h_m/T_s + \mathrm{d}S_{gen}/\mathrm{d}t + AV\omega/T_s \quad (2a)$$

at steady state $\mathrm{d}S_{cv}/\mathrm{d}t = 0$ and

$$\mathrm{d}S_{gen}/\mathrm{d}t = AV\Delta h_{sl}\{(1/T_s - 1/T_l) - \omega/T_s\} \quad (2b)$$

The first two terms on the RHS of Eq. 2a are the entropy flow out of the CV by *heat and mass flow* crossing the exit and inlet boundaries. The last term is the rate of excess defect entropy crossing the boundary. T_{av} is a isotherm between T_s and T_l. The entropy is balanced by assuming that some of the heat was converted to work of forming defects and assuming $\omega/T_{av} \approx \omega/T_s$ as the entropy per unit volume of the solid associated with such defects. For some of the calculations below $T_l \sim T_m$. By formulating the two balances in this manner we have been able to overcome the lack of knowledge of Δh_m. Accurate numbers for Δh_m are generally not available from experiments and hence Δh_{sl} is employed instead. Equation 2a, though simple is also able to handle any short range order in the liquid that enters the control volume or any metastable phase inside the CV [120, 122].

[4] Note that the entropy rate balance is normally written as $\underbrace{\frac{\mathrm{d}S_{cv}}{\mathrm{d}t}}_{\text{rate of entropy change}} = \underbrace{\sum_j \frac{\dot{Q}_j}{T_j} + \sum_i \dot{m}_i s_i - \sum_e \dot{m}_e s_e}_{\text{rates of entropy transfer}} + \underbrace{\dot{\sigma}_{cv}}_{\text{rate of entropy production}}$ where the Q/T is the entropy exchange at the boundaries. The symbols $\mathrm{d}S_{gen}/\mathrm{d}t$ and σ' are both used in the literature for entropy production rate. In this article $\mathrm{d}S_{gen}/\mathrm{d}t$ is preferred for descibing entropy production rate for the moving control volume at steady state.

[5] In the casting literature Δh_{sl} is given the convention of being positive for freezing, whereas, in the thermodynamic literature it is given a negative sign for freezing. In this article, the convention chosen is from the casting literature, i.e. positive, Δh_{sl} for freezing. Equilibrium entropy of freezing, therefore, follows the same convention. All other thermodynamic variables have the regular thermodynamic conventions.

The energy term ω may be further distributed between the crystalline *microstructure* defect entropy ω' and the lattice disorder excess entropy ϕ_{gl}, both per unit volume leaving the exit face of the CV:

$$\omega = \omega' + \phi_{gl} \tag{3}$$

ω' is the disorder energy associated with common defects in crystalline materials such as grain boundaries, dislocations, etc. [52, 68, 114, 115, 120–123, 127, 128]. The term ϕ_{gl} in Eq. 3 has lattice origins, including residual elastic energy oscillations. For commonly encountered metallic crystalline cellular or dendritic solidification, ϕ_{gl} is zero and $\omega = \omega'$.

The work done per unit volume ω can also be approximated by a dominant defect energy like an area fault energy (Eq. 4), ignoring the smaller energy containing line defects and point defects. The work done W (J), and power output dW/dt (J/s), by the system is considered positive as per the normal thermodynamic convention when the system does work. Work is done by the system to form defects, i.e., the residual boundaries between neighboring cells or dendrites. The power output may be written in terms of the defect energy created:

$$dW/dt = -A\left[V \cdot \gamma_{gb} \cdot (1/\lambda)\right] \tag{4}$$

where γ_{gb} and λ are the grain boundary energy (J/m^2) and the average grain boundary spacing (m), i.e., wavelength of cells or dendrites, respectively, created in the in the solid that leaves the control volume at the exit (see Fig. 1 for examples of such boundaries between individual cells or dendrites).

In the rest of this section the assumption is $\phi_{gl} = 0$. However, if $\Delta h_{sl} \approx 0$, for instance for a second order phase transformation, and if grain boundaries are not formed then it is useful to also consider ϕ_{gl}, a term that represents the increased entropy of a disordered solid over the corresponding crystalline solid at a given average temperature; one that can include for example, a supercooled liquid that can become glass provided [101] $T_s < T_g$ (T_g is the glass transition temperature at the imposed heat removal rate). For a perfectly crystalline solid even with grain boundary defects, $\phi_{gl} = 0$ unless the spacing is so small as to make the grain boundaries interact, in which case the ϕ_{gl} term, is to be also considered.[6] The maximum efficiency of internal transformation-work can never exceed $\{1 - T_s/T_l\}$ for a crystalline solid.

Assume now that a diffuse interface region of dimensions ζ is established during DS for a plane front (PF) morphology. Across this region, entropy is generated by various processes. The terms that can generate entropy are the temperature gradient, the configurational entropy generation terms from solid–liquid *mixing* in the diffuse interface region, the entropy generation by atom transfer in the diffuse zone across a free energy potential and across the activation energy barrier that leads to net increase in the volume fraction of the solid (this is similar to the entropy generation at by a reaction force (affinity $(A_f)/T$), and the corresponding flux in the change in fraction of the solid, and the irreversible entropy generated by the flux–force combinations from other atom or electron movements (i.e., solute flux, vacancy flux or electric current and corresponding forces if present). A bulk solid with no grain boundaries or with only very low energy boundaries such as tilt or twist boundaries with identifiable dislocations, has less excess energy compared to one with high energy grain boundaries for the same defect area. Regardless it should be noted that the defect energy per unit volume is normally less than about 10% of the Δh_{sl} for metals unless rapid solidification conditions are encountered. Entropy generation variations can occur if the free energy curve shown in Fig. 3, with and without defects will modified by any solute ordering or cluster gradations, which redistribute the solid and liquid. For simplicity, a linear temperature-potential gradient in the solid–liquid zone is considered.

The entropy rate balance for a pure material with simple a diffuse planar interface can be performed as shown in Eqs. 2a and 2b. The entropy production (generation) rate from the temperature gradient is $K\{\text{grad}.T/T\}^2$ (J/(m^3 K s)). The entropy production rate from the liquid to solid atom transfer on account of a free energy difference per mole is $-\Delta\mu \cdot v \cdot \varepsilon/(\zeta \cdot T_{avt} \cdot v_m)$ (J/(m^3 K s)). Here T_{avt} is an average temperature between the liquid and solid for that transforming atom location (J/(m^3 K s)). The potential $\Delta\mu$ includes the *complete* potential difference and is the free energy/mole plus other potential differences that need to be captured at temperature T_{avt}, v_m is the molar volume, v is the jump frequency from liquid to solid at the temperature T_{avt} for a mole of atoms, ε the *net* distance moved by the interface when 1 mol of atoms is added to the solid from the liquid and ζ as defined above is the thickness of the interface or mushy zone. References [67, 116, 117] contain detailed discussions on ε and v. Entropy generation is a positive term. The rate of entropy of generation per unit volume from the well mixed of solid and liquid at any scale is $-VR(f_s \ln f_s + f_l \ln f_l) df_s/\zeta$. R is the gas constant in J/K m^3 s (i.e., $R = R_g/v_m$) where R_g and v_m are the universal gas constant and molar volume, respectively). When integrated over the control volume this term is approximately equal to $\sim VR/2\zeta$ (J/m^3 K s), where $\zeta =$ mushy zone length, for cells and dendrites or the diffuse zone for the plane front (PF) conditions. For mushy zones, the exact configurational entropy at steady state may also be calculated by determining the solid fraction from the

[6] One assumption that is made for the model is that the majority of the energy associated with defects is captured in area defects like high angle grain boundaries typically $\sim$100 mJ/m^2. Equation 2b reflects the part of the heat which has been converted to work of creating grain boundaries, within the limitations of the second law.

secondary arm distribution but this could prove to be a complex study when secondary arms are observed.[7] Similarly if dS_{gen}/dt is known as a function of ζ then the secondary arm distribution could be inferred. No such calculations yet exist and so $VR/2\zeta$ will be assumed for the MEPR model. Mushy zones are typically in the order of micrometers and the diffuse interfaces are of the order of nanometers. The total configurational entropy generated (dependent on velocity) is $VRA/2$ where A is the area of the interface and V is the velocity normal to the interface. When considering a very dilute alloy with local equilibrium interface conditions that are reflected in the equilibrium partitioning of the solute between liquid and solid; the solute influence can be reflected simply in the changed T_l and T_s as a first approximation. Alternately, the term shown below in Eqs. 5 and 6 may be used. When considering cells and dendrites, the assumption is that T_s and T_l are the solidus and liquidus, respectively. T_l is likely to remain close to T_m for dilute alloys but T_s will decrease with velocity for an alloy with a negative slope of the liquidus. Additionally a force–flux entropy production from the solute gradient in the liquid can be added, i.e., from a flux of solutes equal to $A{\cdot}D_l{\cdot}C_0(1 - 1/k)/\delta_c$ where δ_c is the solute boundary layer at steady state, approximately equal to $2D_l/V$ and C_0 is the dilute alloy composition in solute moles per unit volume.

We will ignore any entropy generation in the diffuse interface region on account of a possible solute gradient as it is not clear if such a gradient is established. If it existed one could assume that the solute gradient is linear in the mushy zone (an assumption that is clearly unreal but allows considerable simplifications). The solute flux entropy generation condition from this solute gradient inside the interface would then be written as:

$$dS_{gen}/dt = A(-D_{avi}(\Delta C_o/\zeta)\Delta\mu_c/T_{av}) \quad (5)$$

$$\Delta C_o = C_o(1-k)/k$$

$\Delta\mu_c/v_m \approx -RT\ln(1/k)$ for very dilute interstitial solid solutions where k is the partition coefficient at moderate velocities, with a value close to but less than 1. D_{avi} is an average diffusivity. The partition coefficient at equilibrium is determined by the equivalence of the chemical potential in all phases. For large deviations far from equilibrium this partition coefficient will approach 1 [1–4, 68, 122]. When k approaches 1, for example when absolute stability conditions are encountered at very high velocities (order of 0.01–1 m/s), then $\Delta C_o = 0$. The impact of such a high velocity is to generate a considerable amount of entropy which has to be matched by the morphology or lattice defects. At such high velocities note that with increasing velocity the dendrites that form at a low velocity tend to become fine cells and a PF is again expected at the absolute stability velocity [1–4, 10, 24, 66, 68, 72, 124]. If MEPR as a hypothesis is valid, then it must also explain such transitions.

There are many more force–flux relationships that can add to the dS_{gen}/dt. A typical accounting for the rate of entropy generation per unit volume is given in Eq. 3, but the difficulty lies in knowing if all entropy generation terms have been adequately included. Curvature differences [48, 122] lead to entropy generation from flux of atoms with a conjugate force from the difference in curvature. Partition coefficients change between faceted interfaces and curved interfaces [1–4, 14, 123] that can also give rise to flow. The solute flow that is caused by such conditions also produces entropy. Curvature differences especially when the tip radius is very small, i.e., less than 100 micrometers, can also lead to differences in the ordering (both short range in the diffuse interface and long range in the lattice). A potential of order and a curvature will lead to entropy production if there is a corresponding flux. One of the most complex issues facing the accurate application of the Prigogine principle and the MEPR is to know whether or not the most important entropy production combinations have been fully considered at all length scales.

For the one-dimensional steady state heat flow considerations, the entropy generated per unit volume in the diffuse or mushy interface volume, assuming a linear temperature gradient, is $K_{av}(T_l - T_s)^2/(\zeta^2{\cdot}T_{av}^2)$ (J/m^3 K s). Here, T_{av} is the average temperature between T_l and T_s. The subscript (av) refers to an average, and K_{av} is the average thermal conductivity in the zone. Note that certain restrictions are placed on the kinetic constants D_{avi} (m^2/s) and K_{av} (J/m s K). For example K_{av} should *not* be a function of the flux or force but of course may depend on temperature. In this sense, it may be different from commonly reported engineering numbers for the thermal conductivity of a liquid or solid. A proper knowledge of the value of K_{av} is one of the key fundamental difficulties with the approach taken in this article to verify key experimental results. A second order transformation yields a finite but high value of the specific heat (thereby allowing for a high but finite thermal conductivity) *but with no heat production*, as the Δh (enthalpy change) is continuous with temperature for a second order transformation. A first order transformation on the other hand produces heat but the specific heat is unknown at the sharp transformation temperature (i.e., same temperature on the solid and liquid side). This is yet another of the reasons for arguing above that the solidification transformation should be considered as mixed-mode. An approximation is made in this article that crystallization happens continuously in the diffuse zone or mushy zone

[7] Very few reports with the detailed microstructural analysis of this kind made from cross sections obtained from quenched interfaces exist [106, 117, 118].

with the solid fraction increasing continuously from T_l to T_s. It is recognized that the shape of the free energy curve in the diffuse region may cause solid fraction to vary in an abrupt manner and the shape of secondary arms in dendritic solidification may very well also cause such a phenomena (i.e., of solid mixing differences across the mushy zone). Such variations are not considered in any detail except to capture a entropy of mixing. Specific defect generation and flux term exists across the entire diffuse interface, the details are again left to a future discussion. Pathway selections (morphological transitions) now become feasible to explain as a consequence of invoking MEPR.

Regardless of the difficulty in identifying all the terms for entropy generation, several of the main terms can be captured as shown below in Eq. 6a. Equation 6a is an important equation that connects atomistic and molecular processes to morphology. The fourth term on the RHS adds entropy to the CV.

$$\begin{aligned} ds_{gen}/dt = {} & K_{av}(T_l - T_s)^2/\left(\zeta^2 \cdot T_{av}{}^2\right) - \Delta\mu_{sl} \cdot v \\ & \cdot \varepsilon/(\zeta \cdot T_{av} \cdot v_m) + VR/2\zeta \\ & + \left(D_l \cdot C_0(1 - 1/k)\pi \cdot v_m/T_m \cdot \delta_c{}^2\right)\Delta\mu_c + \psi \end{aligned} \tag{6a}$$

The variable ψ is introduced to account for the clubbed force–flux entropy production rate per unit volume not considered in the four terms in Eq. 6a. ψ can contain several additional terms for the entropy generation, e.g., from the spatial gradient of the solute or vacancy potential $\left(M\left(\frac{d\mu}{d\zeta}\right)^2 \cdot \frac{C_{av} \cdot v_m}{T}\right)$ leading to vacancy diffusion (where M is the mobility), and from other defect generation and defect transport terms. ψ can also capture the smaller entropy generating cross terms from thermoelectron fluxes [132], i.e. a thermal force that drives the electron flux and vice versa. Although D_l has been used in Eq. 6a, it can be substituted by D_{avi} for dilute metallic alloys which will be in the order of 10^{-13} m^2/s for diffuse interface conditions and in mushy zones will be in the order of 10^{-9} m^2/s. π is a function of velocity that is 1 for the PF morphology and corrects for the overall flux in front of the curved interface(s) for other morphologies.

By making the substitution that:

$$V = v \cdot \varepsilon \tag{6b}$$

and

$$G_T = (T_l - T_s)/\zeta \tag{7a}$$

The temperature difference is always

$$\Delta T = (T_l - T_s). \tag{7b}$$

$$\begin{aligned} ds_{gen}/dt = {} & K_{av} \cdot G_T{}^2/T_{av}{}^2 - \Delta\mu_{sl} \cdot V/(\zeta \cdot T_{av} \cdot v_m) \\ & + VR/2\zeta + \left(D_l C_0(1 - 1/k)\pi \cdot v_m/T_m \cdot \delta_c{}^2\right)\Delta\mu_c \end{aligned} \tag{8}$$

Equating 2b and 7 yields:

$$\begin{aligned} & AV\Delta h_{sl}[1/T_s - 1/T_m] - AV\omega/T_s \\ & = A\zeta\left\{K_{av}G_T{}^2/\left(T_{av}{}^2\right) - \Delta\mu_{sl} \cdot V/(\zeta \cdot T_{av} \cdot v_m)\right. \\ & \left. + VR/2\zeta + \left(D_l \cdot C_0(1 - 1/k)\pi \cdot v_m/T_m \cdot \delta_c{}^2\right)\Delta\mu_c\right\} \end{aligned} \tag{9a}$$

A few checks with known experimental reports and theoretical predictions can be made at this stage. Equation 9a, generally describes the relationship in the transitional zones including for facet and no-facet transition. The diffuse zone is expected to be in the order of nanometers and mushy zone in the order of microns for this region and depends considerably on the value of D_{avi} which varies between the solute diffusivity in the solid and that in the liquid.[8]

For the condition where: $V\delta_c \sim 2\ D_l$ the critical velocity for interface break down, V_c, can be calculated from the first term of the LHS and last term of the RHS of (9a). This gives

$$V_c \cong 4\left[\frac{\Delta s_{sl}}{R}\right]\left[\frac{1}{(1-k)}\right]\left[\frac{G_T D_l}{\Delta T}\right] \tag{10}$$

Equation (10) is similar to the prediction first made by Chalmers et al. [1–4] for a atomically rough interface. The critical velocity value is modified by the interface diffuseness and other parameters. As discussed below, note that the entropy generation rate is a non-zero constant. Also note that $G_T/\Delta T = 1/\zeta$.

Discussions: Bifurcations, Wavelength of Defects, and Metastable Morphologies

Equations 2a–10 make predictions from the balance of the rate of entropy generation and entropy transfer for steady state conditions. Equation 7 shows that S_{gen} rate change with ζ, and $(T_l - T_s)$, these are opposing influences which means that very atomistically smooth surfaces have higher S_{gen} rate over more diffuse interfaces for similar $(T_l - T_s)$ values when compared at the same velocity. Similarly, between stubby cells and dendrites, the cells will have a higher entropy generation rate as the mushy zone is

[8] There is the possibility that the Cahn [114] diffuseness parameter (g), i.e., the number of diffuse layers; the order parameter used in phase field models [17–24]; and the term α^2/ζ^2 could be connected where α is the lattice parameter. The possibility is left to be studied in the future. See also Tiller [131].

narrower. A higher thermal conductivity or a higher diffusivity will generate more entropy for the same steady state velocity of transformation.

However, several of the constants and their temperature dependence in Eq. 3 are unknown (such as K_{av}, D_{avi}, ν, ε). This is the major drawback for testing for the correctness of the approach. Nevertheless, it is possible to make some general arguments. V impacts the ds_{gen}/dt in a direct manner; increasing V increase the S_{gen} rate. As $(T_l - T_s) = \Delta T$ approaches zero, a first order transformation with an atomically smooth solid–liquid interface is possible to infer from Eq. 3 as this is the same condition that decreases ζ. However, all terms approach zero, for this low velocity plane front and a first order transformation at as V tends to 0 correspondingly dS_{gen}/dt tends to 0.

From an energy balance condition for steady state DS, the term $(-V\Delta h_{sl})$ is also equal to $(-K_s G_{T_s} + K_l G_{T_l})$ at least for high thermal conductivity metallic material solidification. Here, G_T is the process imposed temperature gradient and K is the thermal conductivity, and the subscripts, s and l stand for rigorous solid and liquid, respectively. G_T is the independently established temperature gradient in a DS experiment along with an independently imposed velocity V, of solidification (typically established in Bridgeman crystal growth by external control). The influence of the temperature gradient is to decrease ζ at fixed $(T_l - T_s)$ but the gradient also influences other variables because of coupling. If there is a flow of solute or vacancies (i.e., if Kirkendall type vacancy velocities are established in the solid) there will be additional entropy generation from such flux-conjugate force combinations and from new defects such as porosity all (captured in ψ).

The interface diffuseness also appears to depend on ε, the amount that is moved by the addition of 1 mol of atoms. As the diffuseness dimension approaches a value less than lattice spacing, sharp interfaces are expected. Typically closed packed directions have a lower interface diffuseness compared to less packed directions. If ε is small (for example as seen in the lateral step growth regime, or for small net atom transfer from a very small driving force for solidification compared to RT) the diffuseness can correspondingly be small. If ε is at least of the order of the lattice parameter, the correspondingly diffuseness can be thought to increase in a continuous manner. The Jackson model [66] can also be seen in Eq. 9 and 10 when the value is low for the second term on the RHS of equation 9a. The effect of increasing the velocity V on the diffuseness (see footnote 5), as predicted by Cahn [65], is also noted in a more complex fashion through the ΔT and V relationship. Increasing the velocity of transformation will increase s_{gen} rate. By differentiating the LHS sides of Eq. 9a with respect to velocity (V) the $[d\Delta T/dV]_{T_s}$ is positive and $[d^2\Delta T/dV^2]_{T_s}$ is negative, this ΔT is at the maximum. This is an approximate manner of testing for maximum or minimum in contrast to the strict variational principles that have been used [5–7, 108–112] to prove that the MEPR postulate is valid.

One may now examine if the entropy generation rate is maximized at any given velocity with the morphology that is experimentally observed. When a steady state condition is encountered, the minimum entropy production principle (PPEDMR) makes no further predictions about the nature of the emergent steady state (for multiple flux–force combinations) between the many steady state conditions that are possible [112, 122]. In contrast, MEPR provides a selection principle [112] (see Fig. 4) of the most probable condition between many possible steady states.

The MEPR hypothesis that that the highest s_{gen} rate is possibly predictive of the most stable morphology can be tested by comparing with experiments. A few specific morphologies are discussed below and tested with the hypothesis. Although Eq. 6a contains several variables that are unknown, general observations can be made with respect to morphological bifurcations. These are discussed with the help of Fig. 5 which shows the s_{gen} rate vs. velocity. The maximum work done or power delivered is when S_{gen} and S_{gen} rate is the lowest possible for an open system at steady state. From an energy balance this condition yields;

$$(dW/dt)_{max} = -AV(\Delta h_{sl} - \Delta h_m) \tag{11a}$$

where A is the area of the solidification interface normal to the DS direction.

$$dW/dt = -A\left[V \cdot \gamma_{gb} \cdot (1/\lambda)\right] \tag{11b}$$

$$dS_{gen}/dt = -AV\Delta h_{sl}\{1 - T_l/T_s\}/T_l + (dW/dt)/T_s, \tag{12a}$$

which is the same as Eq. 2a.

$$dS_{gen}/dt = AV\Delta h_{sl}\{1 - T_s/T_l\}/T_s - \left(\gamma_{gb}/\lambda + \tau\right)AV/T_{av}, \tag{12b}$$

if τ is small compared to γ_{gb}/λ, then, the maximum possible work or minimum possible λ (the primary spacing) is given by $dS_{gen}/dt = 0$; which gives

$$\lambda \sim \gamma_{gb}/(\Delta s_{sl} \cdot \Delta T) \tag{13}$$

ΔT is of the order of 1–10 K in very dilute metallic alloys in the cell zone and order of 100 K for dendrites the dendrite root is eutectic temperature. In mushy zones the experimentally recorded order of the spacing is about 10–100 μm when V is in the order of micron/s and G_T is in the order of 10 K/mm. For Al–Cu alloys, λ is predicted by Eq. 13 to be of the order of a nanometer whereas

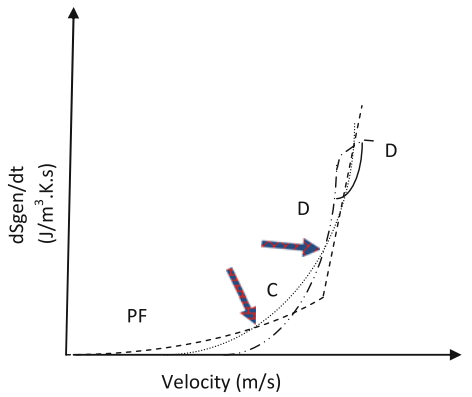

Fig. 5 A schematic plot of S_{gen} rate as a function of the imposed velocity for DS (also the steady state interface velocity). *PF* indicates plane front, *C* indicates cells, *D* indicates dendrites. The MEPR postulate indicates that the maximum rate of entropy production will determine the choice of the most stable pathway (morphology). Note that with increasing velocity, arrays, cells and dendrites will become more stable. The maximum rate of entropy generation will determine the most stable morphology at any imposed steady state velocity. The Prigogine Principle (PPEDMR) predicts the shape of each curve. The light (red) colored arrows point to the most stable PF-C and C-D bifurcations. Note that the possible shape change(s) of the dendrite curve allows for cells or PF to become dominant again at high velocities. At very high velocities (rapid solidification conditions), note that the shape change in the PF curve which can finally lead back to PF as the dominant morphology again depending on the possible slope changes for other morphologies. The kink in the PF curve indicates possible interaction between grain boundaries leading to a higher slope in the S_{gen} rate as a function of velocity

experimental results show it to be much larger [1–4]. Minimum work on the other extreme is the condition when S_{gen}, and dS_{gen}/dt are at maximum for the imposed solidifications conditions (thus establishing the correct λ as a consequence). Maximizing the S_{gen} rate increases λ for a steady state velocity conditions when comparing morphologies with different spacing.

To use MEPR in a normative manner, if dS_{gen}/dt is further differentiated with respect to velocity after setting $ds_{gen}/dt = C$ production, yields:

$$d\ln\lambda/d\ln V = 1 - \left(\lambda\Delta s_{sl}\cdot T_{av}/\gamma_{gb}\cdot T_s\right) \qquad (14)$$

Equation 14 indicates that the slope for dendritic spacing may not be particularly sensitive to velocity for a fixed boundary energy. $d\lambda/dV$ is negative for a Al–2wt% Cu alloy, $d\lambda/dV \sim -1$ which is the order of the measured $d\lambda/dV$ [1–4].

Experimentally, the shapes that are observed with an increase in the velocity above the critical velocity are faceted arrays for a fixed G_T (Fig. 1(a2) or non-faceted arrays such as cells and dendrites Fig. 1c) compared to a plane front which is stable at lower velocities. Equation 14 indicates the direction of $d\lambda/dV$ for a dynamic system where V is varied continuously. Although Soomboonsuk and Trivedi [63] have explored dynamic variations which Eq. 14 is able to predict, there is clearly a need for more experiments to have confidence in Eq. 14 as being predictive for non steady state conditions.

If correct, the MEPR will choose the morphology that has the highest rate of entropy production. Figure 5 (log–log) is a possible schematic plot of ds_{gen}/dt with steady state interface velocity for various morphological features. The system will pick the highest S_{gen} production rate morphology from competing morphologies if MEPR is a correct postulate. Following this approach, the dominant morphological possibilities with MEPR as the governing principle are shown schematically in Fig. 5. To test between a cellular and dendritic morphology for example the maximum ds_{gen}/dt can be calculated by noting that $(T_l - T_s)$ is larger but ζ is also larger for dendrites which will then lead to a result that indicates that a higher spacing can result when a cell to dendrite transition occurs and cells have a possibility of generating more entropy than dendrites at a lower velocity. This is also the experimental observation [63, 106, 117] for DS when a positive temperature gradient is established. When the temperature gradient is negative there appears to be no possibilities where cellular morphologies can have higher rate of entropy generation, as the velocity cannot be independently established when a bath undercooling is fixed.

The many bifurcations corresponding to the sequences shown in Fig. 1 can now be explained with the MEPR postulate. Future publications will address more details and more rigorous tests of the proposed MEPR hypothesis but the preliminary indications are that hypothesis is valid. A plane front (PF) is characterized by no grain boundary production, at least when compared to cells and dendrites. The first break down of a PF to a faceted or non-faceted cell array is a morphological variation method for the system that allows an increase in $(T_l - T_s)$, and thus allows generation of more entropy with a further increase in velocity. This type of reasoning also explains why existing grain boundaries are the first location for interface breakdown. In the PF regime the s_{gen} rate increases with velocity, by enabling entropy generating processes for defect movement. It could be imagined that this is the process that also leads to the initiation of the early perturbations prior to interface breakdown, thus explaining why not much scatter exists for experimentally measured V_c values measured at different magnifications. The PF replacement by stubby cells is enabled when the s_{gen} rate for stubby cell morphology exceeds that for the PF. Note also that the un-mixing (a term that requires work done on the system not work done by the system) in an alloy during steady state solidification is also now spread over the mushy zone. Curvature also creates S_{gen} processes with corresponding curvature induced gradients of solute and

gradients in curvature [48], neither of which are fully captured in Eq. 6.

The cell to dendrite transition with a further increase in velocity is noted with a corresponding increase in spacing before again decreasing the velocity. This condition reflects enhanced entropy generation which is seen in the evolving confused looking mushy zone structures, i.e., those with secondary arms (see Fig. 1), including those in facet forming alloys after tip splitting is no longer possible (due to lack of sharper (111) plane intersections [41]). Experimentally observations showing entropy transitions between tips with different crystallographic axes have been recorded for ammonium chloride dendrites where a (100) dendrite evolves from the more entropy generating (110) dendrite [129]. Nevertheless the precise reason for the selection of specific crystallographic planes during dendritic growth is not yet completely obvious, but seems to have to do with diffuse interfaces and mushy zones to maximise entropy production by (111) planes in face centered cubic materials [1–4, 7, 129]. Curved tips for non-faceted materials and sharp-tips bounding the (111) planes in faceted materials are most likely also a way of maximizing the rate of entropy generation; for a particular T_{av}. For a more detailed explanation, further studies are required. Also note that increasing the velocity at a fixed tip angle can lead to residual stresses and lead to corresponding asymmetric tensile stresses that in turn can cause crack propagation as a way for generating entropy [42]. Residual stresses are a way to store energy thus impacting terms like ω and ϕ. As reported in Refs. [1–4, 10, 41, 63] for faceted and non-faceted materials, for a fixed interface velocity, there are a number competing morphologies available that allow both the coarse morphologies and finer morphologies to co-exist. *These represent mixed (even metastable) morphologies for the imposed sets of processing variables.* Half cells and half dendrites are supported by the MEPR principle. Periodic tip splitting in non-faceted dendrites could reflect adjustment methods of controlling the S_{gen} production for different materials and competing morphologies.

Reducing ζ is a stabilizing influence on PF. Increasing G_T is a stabilizing influence. Both lead to a higher entropy production rate. For kinetic models [1–4] the PF stability comes from the stabilizing influences of the temperature gradient and s/l interface energy. However, this does not address the question of why there is an *overall* morphological stability of one type preferred over another, only that it is feasible. The MEPR appears to solve this problem and possibly explain many of the very complex variations in morphologies, like half cells and half dendrites or half facets shown in Fig. 1. Half cells are a way of supporting a higher entropy rate generation and are seen in both facet arrays [41] and non-facet arrays [69–72].

The growth along closed packed directions is a way of increasing the entropy generation rate as it is a method of reducing the ζ (see also Refs. [7, 112, 129]). When external constraints are introduced, (e.g., as shown in Fig. 1c and d) the energy impact from an external surface influences the entropy production rate. Note that in Fig. 1c from Ref. [70], the higher energy non-wetting surface leads to a much more disorganized looking, half-dendritic (non-crystallographic) pattern whereas the lower energy wetting surface produces a much more regular looking, but non-crystallographic dendrite. Again, using the MEPR principles suggests that an external surface that stabilizes a particular morphological pattern when selecting between several metastable competing morphologies is the one that maximizes the total entropy production rate and therefore is the most favored. By using appropriate constants the entropy rate maximization along with PPEDMR could also possibly reveal fine details, such as explaining why cells are sometimes oval shaped (2D cells) [106, 118] or occasionally five and seven sided cells [119]. These are pathway selection possibilities that are most likely made for optimizing the specific dS_{gen}/dt requirements.

At a high velocity, the conditions for absolute stability [1–4, 10, 24, 66, 68, 72, 124] are encountered. Unfortunately, several of the experimental velocities and other conditions recorded for absolute stability, are not fully tested for an unambiguous steady state behavior. However, assuming that steady state conditions prevail, a few comments can be made about the rate of entropy generation during this high velocity rapid solidification condition. In any case, the work efficiency still cannot exceed $[1 - T_s/T_l]$ during absolute stability conditions. The term neglected in developing Eq. 1a, namely the entire lattice associated constituents of ω, may have to be considered. Regardless, a plane front (PF) can reappear (in preference to very fine cells) at high velocities (rapid solidification conditions) as shown in Eqs. 14–17. Note from Eq. 6a, that a positive temperature gradient allows for the velocity at absolute stability conditions when $\Delta C_0 = 0$, to be slightly lower when comparing with a zero temperature gradient condition in the diffuse region. The main terms at the absolute stability morphological conditions are:

$$AV\Delta h_{sl}[1/T_s - 1/T_l] = A \cdot \zeta\left\{K_{av}G_T{}^2/\left(T_{av}{}^2\right) - \Delta\mu_{sl} \cdot V/(\zeta \cdot T_{av}.v_m)\right\} \quad (15)$$

In the equation above, vacancies have not been considered. The thermodynamics of rapid solidification has been well studied by Kurz, Prigogine and Kondepudi, Aziz, and Baker and Cahn [1, 68, 114, 115, 124] and may be easily incorporated into Eq. 15 for further rigorous development. For an approximate analysis one can consider that $T_{av} = (T_s + T_l)/2$.

If $\Delta\mu_{sl} = \Delta s_{sl}\cdot\Delta T/v_m$ then,

$$\Delta s_{sl}\cdot\Delta T/T_s = \zeta\cdot K_{av}G_T{}^2/V\cdot T_{av} + \Delta s_{sl}\cdot\Delta T_i/T_{av} \qquad (16)$$

If a calculation is performed with values for aluminum, then for a moderate 100 K/mm temperature gradient, a wide diffuse interface of the order of about 1 μm seems possible from Eq. 16, when ΔT is in the order of 1–10 K. Notably $\Delta T \sim \Delta T_i$ at this limit.

Most importantly we note from Eq. 8 that the MEPR model indicates that

$$ds_{gen}/dt = V^2\chi \qquad (17)$$

Where χ is a specific morphology (microstructure) parameter that depends on T_{av} and composition.

Summary, comments, and conclusions

The maximum entropy production rate (MEPR) as a postulate for steady state directional solidification is offered as a postulate for the prediction of the stability of any particular class of morphology (patterns) over other competing types. Wherever work is done during a phase transformation, i.e., when there is a change in free energy between the various phases, the MEPR is a more powerful hypothesis compared to the PPEDMR, as it allows a pathway selection principle which identifies the exact work done, compared to the total work potential. Consequently the corresponding dissipative shapes may be identified. When $ds_{gen}/d(\text{flux}) = 0$, which is a condition very close to the Onsager linear regime [132], both the MEPR and PPEDMR converge. Within a class of morphology, the MEPR is also able to predict the fineness of a structure with changes in the imposed conditions, like the imposed solidification velocity or temperature gradient. Therefore, the MEPR approach may become an important single parameter method for assessing the morphological stability, with applicability over the entire range of solidification morphologies in an analogous fashion to free energy when employed for understanding the thermodynamic phase stability.

This article employs the energy and entropy balance approach for discussion of the MEPR as being deterministic of the most stable pattern in the solid–liquid region formed during solidification. The model does not change any predictions made by the kinetic approaches that have been successful in the past (see, e.g., the first four references cited as Refs. [1–4]); in fact relying on them and the many published experimental observations to validate the MEPR hypothesis. Kinetic approaches are able to find a stable feature of the observed morphology, (e.g., the interface break down condition for a plane front interface) or the conditions for predicting the tip radius from the tip stability parameters for a dendrite. If the MEPR had to be used independently, either all the force–flux conditions would have to be known or all possible shapes have to be tested against each other to predict the most stable morphology. Regardless, with the MEPR, the experimental observations of stable shapes may be validated by comparing against other shapes. The predictions of cellular morphologies and the conditions for cell to dendrite transformation have remained elusive to the kinetic models. The MEPR is seemingly able to explain the experimentally recorded morphologies, especially over other competing morphologies across all conditions of solidification.

It should, however, be noted that the tests offered for assessing the MEPR hypothesis in this article are not yet comprehensive, and considerable work needs to be done in the future for confidence, especially when relating to non-steady state conditions. As schematically shown in Fig. 5, the following bulleted sequences summarize the gamut of morphologies that are predicted as a consequence of the MEPR for DS. Particular features may be suppressed or enhanced depending on the alloy and imposed temperature gradient.

- At extremely slow solidification velocities there is no S_{gen} indicated. As the velocity approaches zero there is no work possible. The plane front orients in a direction that allows the maximum s_{gen} rate for very low velocities.
- Residual strain build-up can be the cause for periodic S_{gen} releases by crack propagation or nucleation events.
- Diffusenesses of the interface can vary with an increase in the velocity.
- Half facet cells of a larger spacing can accommodate the increasing s_{gen} rate requirements with a further increase in velocity. This is found especially in a translational regime prior to possible reduction in spacing and/or increase in the tip to root temperature difference.
- With a further increase in velocity, fine facet arrays and half-facet cells can form. Secondary facet formation can further increase the s_{gen} rate.
- Perturbations can form at existing defects in order to increase the s_{gen} rate. Such perturbations may also lead to the reduction of earlier stage defect generation.
- Break down into wavy patterns (stubby cells and later deep cells) will follow for accommodating the further entropy generation requirements with an increase in the velocity.
- Dendrite formation reduces the work done by increasing the primary spacing compared to cells. The dendrites also align to defined orientations. Within a morphology-type, an increase in velocity, leads to finer

primary spacing and secondary arms develop for higher entropy generation variations in the mushy zone.

- A plane front is re-established at extremely high velocities. s_{gen} can be maximized by eliminating all the work required to be done by the system to form finely spaced intercellular boundaries. These conditions also appear to support a very wide diffuse interface.

However, it is clear that there are a number of parameters that are 'adjustable' in order to make such predictions with confidence (this is also the case for the kinetic models). The author recognizes this dilemma while also recognizing, in a positive sense, that the proposed MEPR model appears to describe many of the morphological transitions observed. The maximum rate of entropy generation principle may also able to provide valuable connections between the now experimentally recognized [8–10, 36–42, 84–96, 105, 131], and theoretically anticipated [8, 32–36, 108, 114, 125–130] nano-scale activity, within the larger microstructural features (shapes) that form during solidification and other material processing methods.

Acknowledgements I am grateful to Professor R. Trivedi (Iowa State University, Ames, US), Professor R. Abbaschian (now at the University of California, Riverside US), who greatly helped with my M.S. thesis work in 1978, Professor R. Mehrabian (US), Professor Wilfried Kurz (EPFL, Lausanne, Switzerland), Professor H. P. Li (NTSU, Taiwan), and Professor V. Kuppa (University of Cincinnati, US) for discussions. It should, however, be noted that they have not particularly embraced or discarded this view of solidification morphology. Professor Leon Shaw (University of Connecticut, US) was more than patient and very helpful with the review for this article to be completed for the special publication issue; for this I express my sincere thanks while wishing Professor Abbaschian the best for an equally productive four more decades.

References

1. Kurz W, Fisher TJ (2003) Solidification. Trans Tech Publications, Switzerland
2. Chalmers B (1964) Principles of solidification. John Wiley & Sons, New York
3. Flemings MC (1974) Solidification processing. McGraw Hill, New York
4. Solidification, ASM, Metals Park (1971)
5. Kirkaldy JS (1992) Rep Prog Phys 55:723
6. Venugopalan D, Kirkaldy JS (1984) Acta Metall 32:893
7. Martyushev LM, Seleznev VD (2006) Phys Rep 426:1
8. Boettinger WJ, Coriell SR, Greer AL, Karma A, Kurz W, Rappaz M, Trivedi R (2000) Acta Mater 48:43
9. Sekhar JA, Trivedi RK (1989) J Mater Sci Eng A114:133
10. Trivedi RK, Sekhar JA, Seetharaman V (1989) Metall Trans 20A:769
11. Trivedi RK, Kurz W (1994) Acta Metall Mater 42(1):15
12. Trivedi RK, Magnin P, Kurz W (1987) Acta Metall 35:971
13. Zener C (1946) Trans AIME 167:550
14. Dash WC (1958) J Appl Phys 29:736
15. Wheeler AA, Boettinger WJ, McFadden GB (1993) Phys Rev E 47:1893
16. Ben-Jacob E (1993) Contemp Phys 34:247
17. Ben-Jacob E, Garik P (1990) Nature 343:523
18. Ziegler H (1963) In: Sneddon IN, Hill R (eds) Progress in solid mechanics, vol 4. North-Holland, Amsterdam
19. Debierre JM, Karma A, Celestini F, Guerin R (2003) Phys Rev E 60:4160
20. Suzuki T, Kim SG, Kim WT (2007) Mater Sci Eng A 449:99
21. Goss AJ, Benson KA, Pfann WG (1956) Acta Metall 4:332
22. Boettinger WJ, Warren JA (1999) J Cryst Growth 200:583
23. Boettinger WJ, Warren JA (1995) Acta Metall Mater 43:689
24. Mullins WW, Sekerka RF (1964) J Appl Phys 35:444
25. Langer JS, Müller-Krumbhaar H (1978) Acta Metall 26:1681
26. Langer JS (1980) Rev Mod Phys 52:1
27. Akamatsu S, Faivre G, Ihle T (1995) Phys Rev E 51:4751
28. Xiao RZ, Wang ZP, Zhu CS, Li WS (2009) ISIJ Int 49:1156
29. Eggleston JJ, McFadden GB, Voorhees PW (2001) Physica D 150:91
30. Zheng L, An Q, Xie Y, Sun Z, Luoa S (2007) J Chem Phys 127:164503
31. Balikci E, Abbaschian R (2005) J Mater Sci 40(6):1475. doi: 10.1007/s10853-005-0586-y
32. Cahn JW (1961) Acta Metall 9:795
33. Cahn JW, Carter WC (1996) Metall Trans 27A:1431
34. Cahn JW, Fife P, Penrose O (1997) Acta Mater 45:4397
35. Allen SM, Cahn JW (1979) Acta Metall 27:1085
36. Cahn JW, Hilliard JE (1959) J Chem Phys 31:688
37. Sekhar JA, Rajasekharan TA (1986) Nature 320:153
38. Pellegrini PW, Hutta JJ (1977) J Cryst Growth 42(12):536
39. Rao KN, Sekhar JA (1987) Scripta Metall 21:805
40. Rajasekharan T, Sekhar JA (1986) Scripta Metall 20:235
41. Dey N, Sekhar JA (1993) Acta Metall Mater 41(2):409
42. Dey N, Sekhar JA (1993) Acta Metall Mater 41(2):425
43. Reddy GS, Sekhar JA (1985) J Mater Sci 20:3535. doi: 10.1007/BF01113760
44. Sekhar JA (2001) Metall Trans 32B:1213
45. Sekhar JA, Bharti A, Trivedi RK (1989) Metall Trans A 20A:2191
46. Basu B, Sekhar JA, Schaefer RJ, Mehrabian R (1991) Acta Metall Mater 39(5):725
47. Lin CS, Sekhar JA (1994) J Mater Sci 29:3637. doi: 10.1007/BF00357329
48. Sekhar JA (2002) Acta Mater 50:4841
49. Roosz A, Rettenmayr WatringD (eds) (2000) Solidification and gravity 2000. Trans Tech Publications, Switzerland
50. National Research Council (NRC), Space Studies Board, The National Academies Press, 2005/2006. www.nap.edu
51. (2003) Assessment of Directions in Microgravity and Physical Research at NASA, National Research Council of the National Academies, Washington, DC
52. Watanabe T, Sugiyama Y (2004) J Jpn Inst Light Metals 54(7):293
53. Matsuura K, Kudoh M, Kinoshita H, Takahashi H (2002) Metall Mater Trans A 33A:2074
54. Hillert M (2001) Acta Mater 49:2491
55. Ginzburg VL, Landau LD (1950) J Exp Theor Phys 20:1064
56. Hilliard JE (1970) Phase transformations. American Society of Metals, Metals Park, OH, p 497
57. Sekhar JA, Li HP, Dey GK (2010) Acta Mater 58:1056
58. Knobloch E (1986) Phys Rev A 34(2):1538
59. Saito T, Furuta T, Hwang JH, Kuramoto S (2003) Science 300:464
60. Köehler JM, Müeller SC (1995) J Phys Chem 99:980
61. Lakshmikantha MG, Bhattacharya A, Sekhar JA (1993) Metall Mater Trans A 23A:23

62. Beckermann C (2002) Inter Mater Rev 47(5):243
63. Somboonsuk K, Trivedi R (1985) Acta Metall 33(6):1051
64. Losert W, Shi BQ, Cummins HJ (1998) Proc Natl Acad Sci USA 95(2):431
65. Cahn JW (1960) Acta Metall 8:554
66. Jackson KA (1958) In: Doremus RH, Roberts BW, Turnbull D (eds) Growth and perfection of crystals. Wiley, New York, p 319
67. Cahn JW, Hillig WR, Sears GW (1964) Acta Metall 12:1421
68. Aziz MJ (1982) J Appl Phys 52:1158
69. Fabietti LM, Sekhar JA (1992) J Mater Res 7(8):1987
70. Fabietti LM, Sekhar JA (1994) J Mater Sci 29:473. doi: 10.1007/BF01162509
71. Fabietti LM, Sekhar JA (1993) Metall Trans 23A:3361
72. Sekhar JA (1982) Ph.D. Thesis, University of Illinois
73. Sekhar JA, Trivedi R (1991) Mater Sci Eng A 147(1):9
74. Sekhar JA, Trivedi R (1990) In: Rohatgi P (ed) Solidification of metal matrix composites. ASM, Materials Park, p 39
75. Morris LR, Winegard WC (1969) J Cryst Growth 6:61
76. Barsdley W, Boultton JS, Hurle DTJ (1962) Solid State Electron 5:395
77. Saratovikan DD (referenced from MC. Flemings Solidification Processing, McGraw Hill 1974) (original reference in Russian, Dendritic Solidification, translated by Bradley JES, Consultant Bureau, NY, 1959)
78. Schaefer RJ, Glicksman M (1970) Metall Trans 1:1973
79. Li HP, Sekhar JA (2009) Acta Mater 57:5430
80. Tabony J (2006) Biol Cell 98:589. doi:10.1042/BC20050086
81. Inatomi Y (2009) Journey to Kibo. Experiment on mechanism of faceted cellular array growth, chapter 10. Institute of Space and Astronautical Science/JAXA
82. Prigogine I, Nicolis G (1971) Q Rev Biophys 4:107
83. Prigogine I, Stengers I (1984) Order out of chaos: man's new dialogue with nature. Bantam Books, New York
84. Turing AM (1952) Philos Trans R Soc Lond 237:37
85. Li HP, Sekhar JA (2009) Int J Selfpropag High Temp Synth 18(4):219
86. Kaukler WF, Rosenberger F, Curreri PA (1997) Metall Mater Trans A 28A:1705
87. Kuo C-G, Chao C-G (2007) Int J Adv Manuf Technol 32:468. doi:10.1007/s00170-005-0361-x
88. Dey GK (2003) Acta Mater 51:2549
89. Papp Z, Beke DL, Catanona GL, Langer GA (2003) In: Beke DL, Szabo IA (eds) Defect and diffusion forum, vols 216–217. Trans Tech Publications, Zurich, Switzerland, p 1
90. Maselko J (1996) Mater Sci Eng C 4(3):199
91. Glotzer SC, Di Marzio EA, Muthukmaran M (1995) Phys Rev Lett 74(11):2034
92. Carpenter M (1981) Am Mineral 66:553
93. Lesoult G (2005) Mater Sci Eng A 413–414:19
94. Ohnaka I (1998) Microsegregation and macrosegregation, metals handbook: vol. 15 casting. ASM International, Materials Park, p 136
95. Wu M (2005) Adv Eng Mater 7(9):846
96. Anathakrishna G (2007) Phys Rep 440:113
97. Civitonovic P (ed) (1984) Universality in Chaos, Adam Hilger Ltd, Bristol
98. Gumennyk K, Stefanovich L, Feldman E (2009) Phys Status Solidi B. doi:10.1002/pssb.200844277
99. Kirkaldy JS (1997) Scripta Metall 37(2):125
100. Cahn JW, Novick-Cohen A (2000) Acta Mater 48(13):3425
101. Sekhar JA, Risbud SA (1982) J Non Cryst Solids 47(3):363
102. Reguera D, Schmid G, Burada PS, Rubi JM, Hanggi P (2006) Phys Rev Lett 96:130603
103. Rivier N, Duffy DM (1982) J Phys C 15(3):2867
104. Maraşl N, Keşlioğlu, Arslan B, Kaya H, Çadırlı E (2008) J Mater Process Technol 202(1–3, 20):145
105. Valiev RZ, Estrin Y, Horita Z, Langdon TG, Zechetbauer MJ, Zhu YT (2006) J Miner Met Mater Soc 58(4):33
106. Ho CT, Cheng CJ, Sekhar JA (1991) Metall Mater Trans A 22:225
107. Sato K, Tagawa K, Inoue Y (1991) Metall Trans 21A:5
108. Chandrasekhar S (1961) Hydrodynamic and hydromagnetic stability. Oxford University Press, Clarendon, Oxford
109. Jaynes ET (1980) Annu Rev Phys Chem 31:579
110. Salamon P, Hoffmann KH, Schubert S, Stephen Berry R, Andresen B (2001) Non Equilib Thermodyn 26:73
111. Martyushev LM, Nazarova AS, Seleznev VD (2007) J Phys A 40:371
112. Klaidon Axel (2009) Naturwissenschaften 96:653
113. Peteves SD, Abbaschian GJ (1986) J Cryst Growth 79(1–3):775
114. Tyokodi RJ (1967) Thermodynamics of steady state. MacMillan, New York
115. Kondepudi D, Prigogine I (1998) Modern thermodynamics: from heat engines to dissipative structures. Wiley, New York
116. Jiao YN, Takanori S, Ohsawa Y, Arakane G, Sato A (2000) Mater Res Soc Symp Proc 580:333
117. Tiwari SN, Shah R, Song H (1994) Mater Metall Trans A 25A:535
118. Ojha SN, Tewari SN (2004) Trans IIM 57(5):475
119. Chadwick GA (1967) In: Zeif M, Wilcox WR (eds) Fractional solidification. Marcel Dekker Inc, New York, p 113
120. Ramakrishnan TV (1985) Liquid to solid transformation, materials science forum, vol 3. Trans Tech Publications Ltd, Switzerland, p 7
121. Langer JS, Müller-Krumbhaar H (1978) Acta Metall 26(11):1681
122. Ballufi RW, Allen MA, Carter WC (2005) Kinetics of materials. Wiley, New York
123. Glicksman M (1971) In: Solidification. ASM, Metals Park, p 111
124. Baker JC, Cahn JW (1971) In: Solidification. ASM, Metals Park, p 21
125. Brener EA, Melnikov VI (1991) Adv Phys 40:53
126. Emmerich H (2003) The diffuse interface approach in materials science. Springer-Verlag, Berlin, Heidelberg, New York ISBN 3-540-00416-5
127. Kuppa V, Manias E (2003) J Chem Phys 118(7):2423
128. Kuppa V, Menakanit S, Krishnamuty R, Manias E (2003) J Polym Sci B 41:3285
129. Bejan A (2006) Advanced engineering thermodynamics, 3rd edn. Wiley, New York
130. Hill A (1990) Nature 348:426
131. Tiller WA (1971) In: Solidification. ASM, Metals Park, OH
132. Onsager L (1996) In: Hemmer PC, Holden H, Kjelstrup Ratkje S (eds) With commentary, World Scientific Series in 20th Century Physics, vol 17. World Scientific Publishing, Singapore, New Jersey